Article

Photonic flatband resonances for free-electron radiation

https://doi.org/10.1038/s41586-022-05387-5

Received: 7 October 2021

Accepted: 26 September 2022

Published online: 4 January 2023

Check for updates

Yi Yang[1,2,6]✉, Charles Roques-Carmes[1,6]✉, Steven E. Kooi[3], Haoning Tang[4], Justin Beroz[1], Eric Mazur[4], Ido Kaminer[5], John D. Joannopoulos[1,3] & Marin Soljačić[1,3]

Flatbands have become a cornerstone of contemporary condensed-matter physics and photonics. In electronics, flatbands entail comparable energy bandwidth and Coulomb interaction, leading to correlated phenomena such as the fractional quantum Hall effect and recently those in magic-angle systems. In photonics, they enable properties including slow light[1] and lasing[2]. Notably, flatbands support supercollimation—diffractionless wavepacket propagation—in both systems[3,4]. Despite these intense parallel efforts, flatbands have never been shown to affect the core interaction between free electrons and photons. Their interaction, pivotal for free-electron lasers[5], microscopy and spectroscopy[6,7], and particle accelerators[8,9], is, in fact, limited by a dimensionality mismatch between localized electrons and extended photons. Here we reveal theoretically that photonic flatbands can overcome this mismatch and thus remarkably boost their interaction. We design flatband resonances in a silicon-on-insulator photonic crystal slab to control and enhance the associated free-electron radiation by tuning their trajectory and velocity. We observe signatures of flatband enhancement, recording a two-order increase from the conventional diffraction-enabled Smith–Purcell radiation. The enhancement enables polarization shaping of free-electron radiation and characterization of photonic bands through electron-beam measurements. Our results support the use of flatbands as test beds for strong light–electron interaction, particularly relevant for efficient and compact free-electron light sources and accelerators.

The interaction between free electrons and optical environments gives rise to a multitude of radiative processes[6,7,10,11]. These processes constitute an invaluable diagnostic platform, however, usually at low coupling strength, because of the limited interaction cross-section. Accordingly, longer interaction lengths in extended structures can achieve a stronger coupling strength with quantum vacuum in the spontaneous regime, as studied in photonic crystals[12–18], fibres[19] and plasmonics and metamaterials[20–25]. Such a spontaneous coupling strength, described by the dimensionless g_{Qu} parameter in recent theoretical works[26,27], is also the pivotal benchmark for stimulated processes, as exemplified by a thousand-photon stimulated emission and absorption by a single electron[28] and thousand-electronvolt acceleration[8,29] in extended structures.

The key rule depicting the interaction between free electrons and light is phase matching[10,11]: it requires that the electron velocity $\mathbf{v}$ and the photon phase velocity $\omega/\mathbf{k}$ together satisfy $\omega = \mathbf{v}\cdot\mathbf{k}$. Importantly, the phase-matching condition involves only the longitudinal momentum of the emitted radiation. There remains a continuum of transverse momenta simultaneously allowed in the emitted field. However, photonic modes are not necessarily supported at all of these momenta, which results in a transverse momentum mismatch. Previous proposals for emission improvement either hinge on the hard-to-create sheet-beam excitation (Methods and Supplementary Section 8) in the two-dimensional approximation[16,20] or remain limited to a single transverse momentum in the full three-dimensional setting[17]; in both cases, the transverse momentum mismatch remains, thereby limiting the available enhancement.

This mismatch puts a limit on all conventional free-electron radiation mechanisms. To start, consider the quintessential Cherenkov and Smith–Purcell effects. Free charged particles, such as electrons, generate Cherenkov radiation if their velocity v exceeds the phase velocity of light $c/\sqrt{\epsilon}$ in a homogeneous medium with permittivity ε (Fig. 1a, left). They can also generate Smith–Purcell radiation near periodic structures through near-field diffraction (Fig. 1a, right). Assuming that an electron propagates in the x direction (that is, $\mathbf{v} = v\hat{\mathbf{x}}$), its external fields obey $\omega = v(k_x - 2n\pi/a)$ (referred to as the electron surface hereafter; green surfaces in Fig. 1b), in which a is periodicity, $n = 0$ for Cherenkov radiation, and $n \in \mathbb{Z}_{\neq 0}$ is the diffraction order for Smith–Purcell radiation. In cylindrical coordinates (x, ρ, ψ) in which k_x and $k_\rho\hat{\rho} = k_y\hat{y} + k_z\hat{z}$ are momenta parallel and perpendicular to the electron velocity, respectively, the intersections between the electron surfaces and the light cone $\omega = ck/\sqrt{\epsilon}$ (purple in Fig. 1b) dictate the dispersion relations of both types of radiation. Specifically, Cherenkov radiation is spectrally continuous whereas Smith–Purcell radiation forms

[1]Department of Physics and Research Laboratory of Electronics, Massachusetts Institute of Technology, Cambridge, MA, USA. [2]Department of Physics, University of Hong Kong, Hong Kong, China. [3]Institute for Soldier Nanotechnologies, Massachusetts Institute of Technology, Cambridge, MA, USA. [4]Harvard John A. Paulson School of Engineering and Applied Sciences, Harvard University, Cambridge, MA, USA. [5]Department of Electrical and Computer Engineering, Technion-Israel Institute of Technology, Haifa, Israel. [6]These authors contributed equally: Yi Yang and Charles Roques-Carmes. ✉e-mail: yiyg@hku.hk; chrc@mit.edu

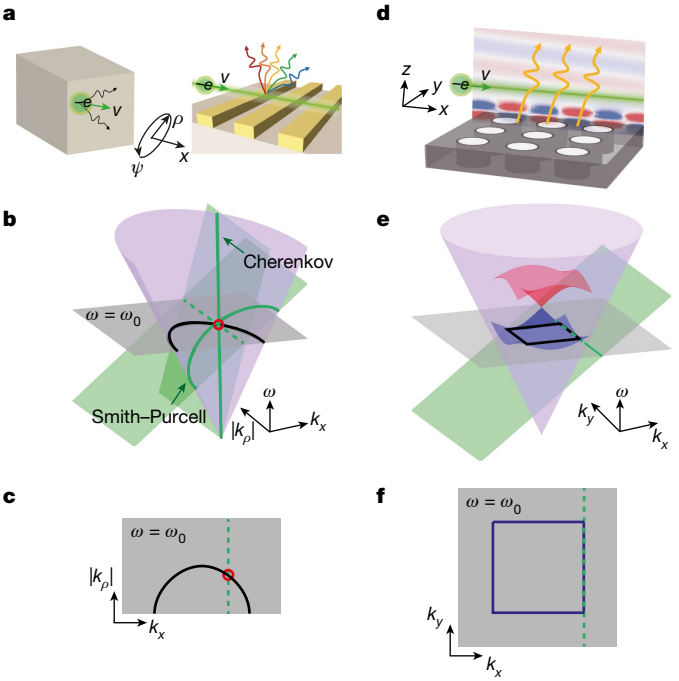

Fig. 1 | Flatband-resonance-mediated free-electron radiation. a, Conventional effects of free-electron radiation. Free electrons in a bulk medium emit Cherenkov radiation when satisfying the superluminal condition (left) or emit Smith–Purcell radiation through diffraction from periodic structures (right). **b**, In momentum space, Cherenkov and Smith–Purcell radiation occur at frequencies and momenta at which the light cone (purple; $\omega = ck/\sqrt{\epsilon}$) and the electron surface (green; $\omega = v(k_x - 2n\pi/a)$) intersect. **c**, At a specific frequency $\omega = \omega_0$, their intersection is always a point degeneracy (red circle), which corresponds to the Cherenkov cone or the Smith–Purcell dispersion relation. **d**, By leveraging resonances in photonic crystal slabs, free-electron radiation can be substantially modified and enhanced. **e**, As the transverse momentum (green line on green surface) of the electron surface is unbounded, a continuum of flat resonances (dark blue square on the light blue surface) can be particularly useful for maximizing free-electron–light interaction. **f**, At a certain velocity and frequency, a line degeneracy exactly at the flatband can be formed between the photonic bands and the electron surface.

discrete spectral windows under various diffraction orders (Fig. 1b). However, in both cases, emission at each frequency ω_0 can occur only at discrete momenta; that is, the phase-matching condition is satisfied only at point degeneracies (red circle in Fig. 1c) between the electron surface and the isofrequency contour. Such nonresonant bare point degeneracies are not optimal for maximizing electron–light interaction. To go beyond that, one can introduce resonant point degeneracies formed with photonic guided modes or resonances and couple them with free electrons to improve the interaction[16–21].

We propose to create higher-dimensional degeneracies in momentum space (that is, line degeneracies) between the electron surfaces and a continuum of photonic resonances to further enhance their interaction. Such conditions can be met by considering the interaction between free electrons and photonic flatband resonances. In particular, we show that the strength of the interaction is intuitively proportional to the Purcell factor and the spectral density of states, both projected along the transverse direction (see derivations in Supplementary Section 6); evidently, a continuum of flatband resonances can simultaneously improve both quantities. Akin to our proposal here, it was previously theoretically predicted that radiated power enhancements could occur near discrete momenta at which the transverse component (orthogonal to the electron trajectory) of group velocity vanishes[30]. Beyond discrete momenta, flatbands naturally satisfy this condition over a wide momentum bandwidth that should further improve the enhancement. We consider Smith–Purcell radiation from a photonic crystal slab that hosts flatband resonances, as shown in Fig. 1d. For conceptual clarity, we first ignore its non-Hermiticity and discuss the band structure of its Hermitian counterpart that is continuously translationally invariant along the z direction. Near the centre of the Brillouin zone (Γ point), the photonic crystal supports bands that can be described by an effective two-dimensional, square-lattice, Dirac Hamiltonian[31]

$$h(k_x, k_y) = \omega_d\sigma_0 + v\sin k_+\sigma_x + v\sin k_-\sigma_y + m\sigma_z, \quad (1)$$

in which ω_d is the frequency of degeneracy, $k_\pm = (k_x \pm k_y)/\sqrt{2}$, σ_0 is the identity matrix, and $\sigma_{x,y,z}$ are Pauli matrices. Its associated bands are shown by the red and blue surfaces above the light cone in Fig. 1e. For negligible mass $m \approx 0$, this Hamiltonian hosts a flatband at $(\omega_0, \mathbf{k}_0)$ (Fig. 1e,f), in which $\omega_0 \equiv \omega_d \pm v$. The isofrequency contour becomes flat, at the critical point between elliptic and hyperbolic dispersions. The frequency of the flatband ω_0 and the size of its contour $\mathbf{k}_0$ can both be tuned by proper design. We need to control simultaneously the velocity of electrons and their in-plane twist angle relative to the photonic crystal (Supplementary Section 9) to realize the desired single-frequency line degeneracy (dashed green–blue line in Fig. 1f) between the electron surface and the flatband. For the flatband perpendicular to the Γ–X direction (Fig. 1f), the optimal twist angle is zero degree. At other non-optimal velocities and twist angles, only point degeneracies can be formed at a single frequency (Supplementary Section 9).

To realize such flatbands experimentally, we designed and fabricated a silicon-on-insulator, square-lattice, photonic crystal slab (Fig. 2a and Methods). We first focus on the lowest, transverse-magnetic-like (H_x, H_y, E_z) band above the light cone whose isofrequency contour is shown in Fig. 2b. A flatband around $\omega_0 \approx 0.287$ (in units of $2\pi c/a$) appears near $|k_x| = k_0 \approx 0.08$ (in units of $2\pi/a$) along the k_y direction and its 90°-rotation partners. In the second Brillouin zone, the overlap between the electron surface and the flatband can appear at $k_x = \mp k_0$, respectively, under two discrete velocities $v_\pm$ in the x direction (Fig. 2b)

$$v_\pm = \omega_0/(1 \mp k_0). \quad (2)$$

Accordingly, radiation towards polar angles $\sin^{-1}\sqrt{k_0^2 + k_y^2}/\omega_0$ and azimuthal angles $\tan^{-1}k_y/k_0$ are selectively enhanced, for which $k_y \in [-k_0, k_0]$ (Supplementary Section 10). The electric mode profiles $|E|$ within a unit cell at ω_0 and $(k_x, k_y) = (k_0, 0)$ are shown in Fig. 2c. As the mode of interest originates from a perturbed guided mode in the slab, it remains mostly confined within the device silicon layer, and the air holes provide external radiative coupling. The existence of the flatband near ω_0 was confirmed with Fourier scattering spectroscopy measurements (Fig. 2d and Supplementary Section 2).

The flatband modifies and enhances free-electron radiation substantially, as shown by the comparison between the simulated radiation patterns and the associated Fourier analysis shown in Fig. 2e–j (see numerical methods in Supplementary Section 7). We identify three regimes of radiation generation. First, at frequencies for which the electron surface is far away from the photonic band (Fig. 2e,f), resonant effects are negligible. Still, radiation is generated by diffraction and allowed towards all transverse directions (Fig. 2f), similar to the conventional Smith–Purcell radiation (Fig. 1b). Second, at frequencies near discrete resonances (that is, point degeneracies between the free electron surface and the photonic band), radiation towards discrete directions gets selectively enhanced. This is confirmed by the associated, discrete Fourier peaks near $|k_y| \approx 0.1$ (Fig. 2h), originating from the tail of a resonance at a lower frequency. Finally, when the electron surface intersects (Fig. 2i,j) the flatband (phase-matching condition shown in Figs. 1f and 2b), enhanced emission is obtained because of the

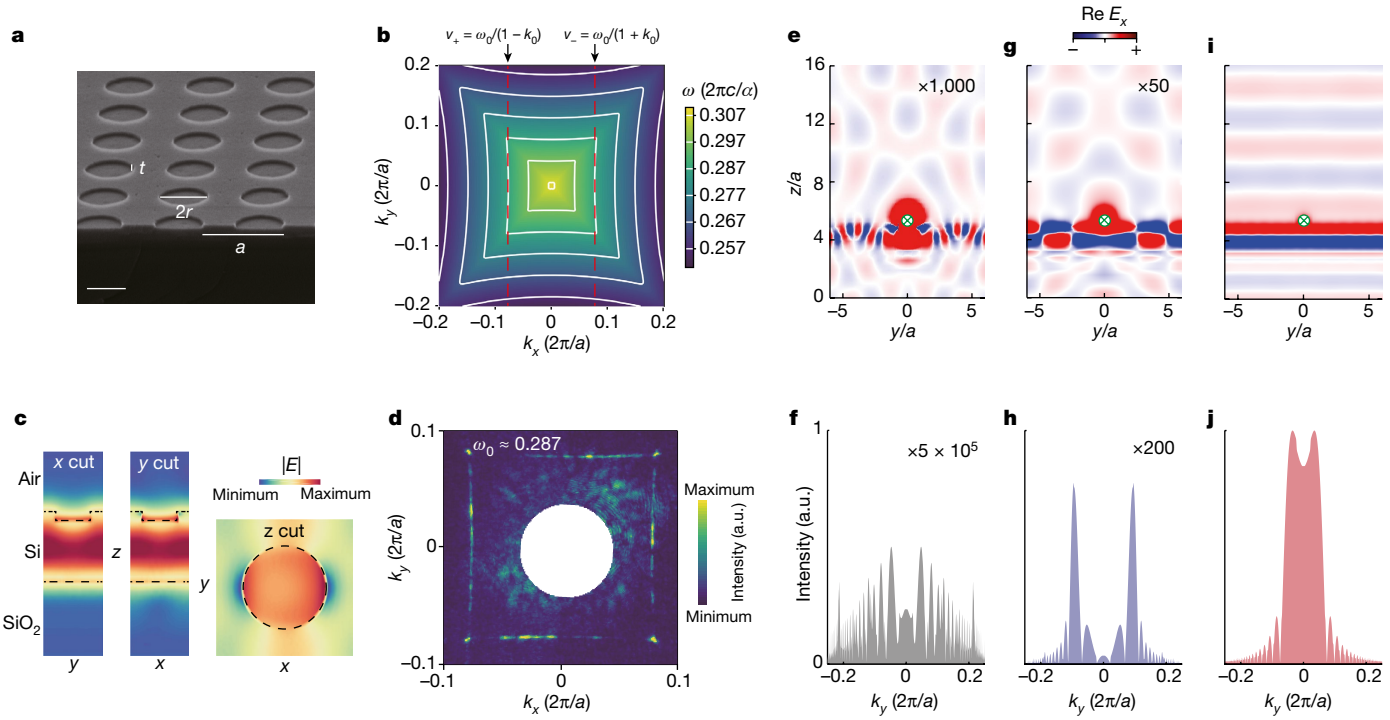

Fig. 2 | Boosting free-electron radiation from photonic flatbands. **a**, A scanning electron micrograph of the photonic crystal slab. Scale bar, 200 nm. **b**, Predicted isofrequency contours. A flatband appears near $\omega_0 \approx 0.287$ and $|k_x| = k_0 \approx 0.08$. Under resonant electron velocities $v_\pm$ (dashed red lines; equation (2)), maximal overlap appears between the electron surface and the photonic band. **c**, Mode profiles of $|E|$ at $(k_x, k_y) = (k_0, 0)$, the centre of the flatband. The *x* and *y* cuts are shown at the centre of the unit cell. The *z* cut is chosen in the middle of the air hole. The dashed lines indicate material boundaries. **d**, Measured isofrequency contours at the flatband (see Supplementary Section 2 for details). a.u., arbitrary units. **e**–**j**, Simulated radiation field profiles Re E_x (**e**,**g**,**i**) and the associated Fourier analysis (**f**,**h**,**j**) when the electron surface is off (**e**,**f**: $v = 0.9v_+$; **g**,**h**: $v = 1.03v_+$;) and on (**i**,**j**; $v = v_+$) the flatband at ω_0. Enhanced radiation can be achieved with the flatband. The green circles indicate the location of the point free electrons. In **e**,**f**, radiation is dominated by diffraction, as indicated by the Fourier components towards all transverse directions. In **g**,**h**, radiation is mainly contributed from discrete resonances at $|k_y| \approx 0.1$. In **i**,**j**, the flatband strongly excites a continuum of Fourier components k_y, which also enable the localization of light (Supplementary Section 11) along the *y* direction despite its extended nature.

excitation of the flatband continuum ($|k_y| \lesssim 0.08$). Such excitation of the flatband also causes localization of light, one of flatbands' hallmark consequences, which we numerically illustrate using the two-dimensional counterpart of our photonic crystal slab in Supplementary Section 11. Taken together, compared to those when the electron surface is off the flatband by 10% (3%), the flatband is predicted to achieve a 1,000-fold (50-fold) field enhancement (that is, a 10^6 (10^3) intensity enhancement). Complementarily, we also numerically compare this flatband-mediated emission with the conventional Smith–Purcell radiation from diffractive gratings (Supplementary Section 12), also exhibiting improvement of many orders of magnitude.

In our experimental setup (Fig. 3a and Supplementary Section 1), 20–40-keV free electrons passed above the photonic crystal at a nonzero grazing incident angle ($\approx 1°$ for targeting and aligning the sample in our setup), which results in the simultaneous presence of Smith–Purcell radiation (Fig. 3b) and incoherent cathodoluminescence[32] (see further discussion below, Fig. 3c and Supplementary Section 5C) in the measured spectra. Meanwhile, this nonzero incident angle caused a few experimental uncertainties (Supplementary Section 5A), chief among which is the increase of free carriers in silicon under electron-beam exposure (Supplementary Section 5B). To account for this, the refractive index of the top silicon layer is chosen as $n_{Si} = 3.2 + 0.03i$ (corresponding to a doping concentration 10^{20}–10^{21} cm^{-3}; Supplementary Section 5B).

At $\theta \approx 0°$ twist angle (Fig. 3d,e), we obtained three experimental signatures of the predicted flatband-enhanced, free-electron radiation. First, both the measurement (Fig. 3e) and the prediction (Fig. 3d) exhibit a region of radiation enhancement near $(v, \omega) \approx (0.35c, 0.285)$ (indicated by white circles) where the electron surface intersects the flatband resonances. Second, we extracted a quality factor $Q_e \approx 50$ from these electron radiation spectra. Although Q_e was lower than $Q_o \approx 400$ from the optical characterization (Supplementary Section 2), owing to the carrier doping from free electrons, Q_e was substantially higher than the 'quality factor' of the conventional Smith–Purcell radiation $Q_{SP} \equiv c/v \approx 3$, and thus indicates the resonant enhancement. Third, in accordance with the simulation taking account of the carrier-induced material loss (Fig. 3b), we obtained a two-order enhancement (Supplementary Section 5D), albeit falling short of the prediction in the ideal lossless situation in Fig. 2. Furthermore, we also experimentally compared the flatband radiation with the conventional Smith–Purcell radiation from a silicon grating (Fig. 3h). Even though the depth of the photonic crystal is about three times shallower than that of the grating, the radiation from the flatband of the photonic crystal is nearly 30-fold stronger than that from the grating.

The measured enhancement region in Fig. 3e is broadened along the velocity axis (Supplementary Section 5C), compared to the idealized Smith–Purcell radiation in which electrons are assumed perfectly parallel to the sample surface (Fig. 3b). As noted above, the grazing-angle electron beam inevitably impinged onto the photonic crystal slab, causing additional radiation pathways[33], predominantly incoherent cathodoluminescence of localized nature, which are far less sensitive to electron velocity than Smith–Purcell radiation but can be simultaneously enhanced by the flatband resonances. We incorporate incoherent cathodoluminescence using a constant Lorentzian fitting (Supplementary Section 5C) across all velocities in Fig. 3c, which achieves improved correspondence between the full theory (Fig. 3d) and the measurement (Fig. 3e).

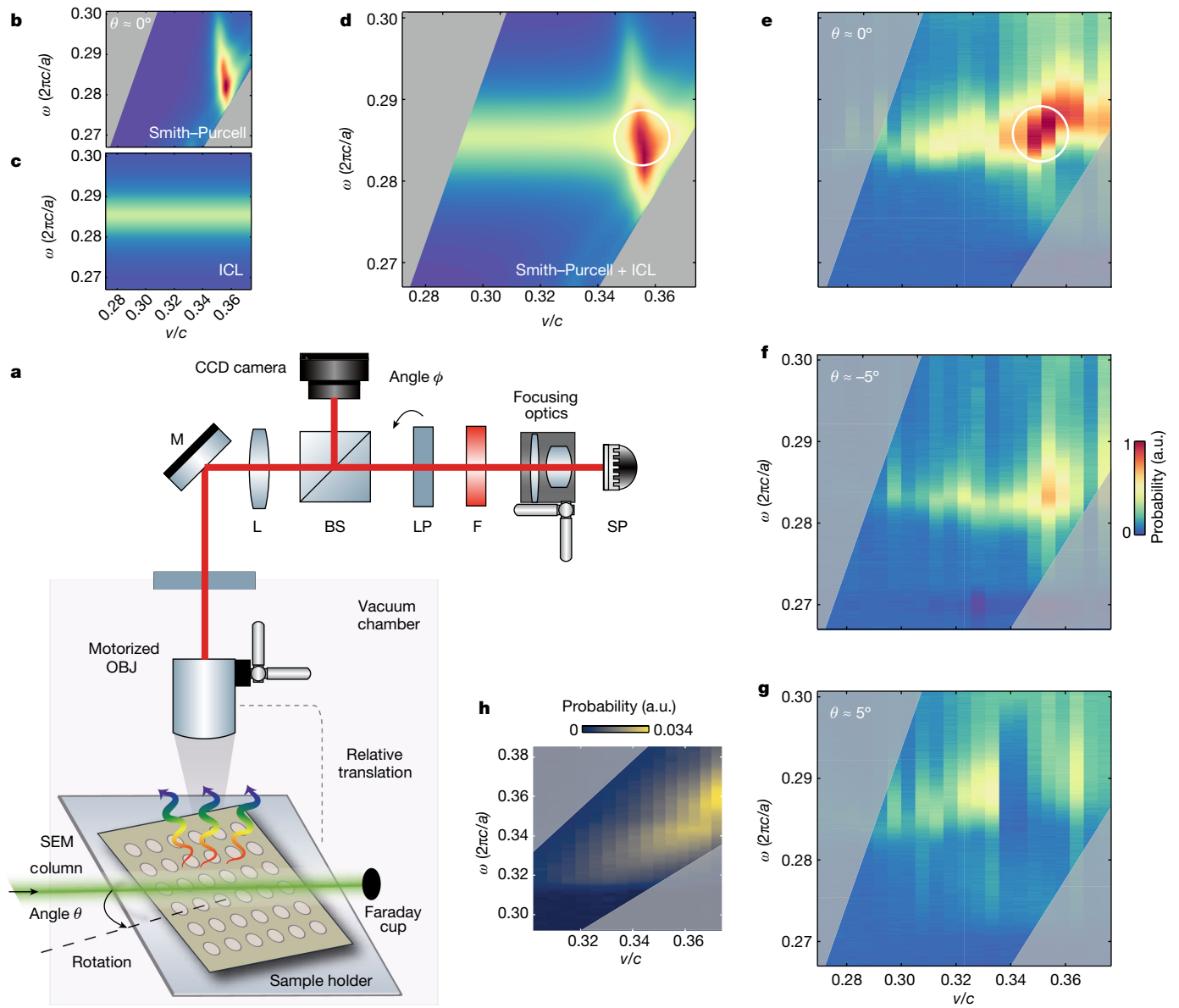

Fig. 3 | Measurement of radiation from flatbands. a, Scanning electron microscope (SEM)-based experimental setup (Supplementary Section 1). Radiation was measured under three in-plane twist angles θ between the electron beam and the photonic crystal slab. The linear polarizer was oriented at angle $\phi \approx 0°$ (that is, parallel to the electron beam), consistent with the far-field polarization of the mode. OBJ, objective; CCD, charge-coupled device; M, mirror; L, lens; BS, beamsplitter; LP, linear polarizer; F, filter; SP, spectrometer. **b**, Numerically calculated Smith–Purcell radiation for point electrons perfectly parallel to the sample surface. **c**, Single Lorentzian fitting of the incoherent cathodoluminescence (ICL), a concurrent radiation pathway under non-parallel electron incidence. **d**,**e**, Theoretical (combining both Smith–Purcell (**b**) and incoherent cathodoluminescence (**c**) emission) (**d**) and measured (**e**) radiation at $\theta \approx 0°$. The signature of flatband resonances is indicated by the white circles, highlighting maximal enhancement. **f**,**g**, Measured incoherent-cathodoluminescence-dominated emission at $\theta \approx \pm 5°$ in-plane twist angles. **h**, Benchmark Smith–Purcell radiation (from a silicon grating with periodicity 500 nm, depth 150 nm, and a duty cycle of 0.44) that is 30-fold weaker than the measured flatband radiation. Shaded areas indicate parameter space outside the numerical aperture of the objective.

We next explore radiation as a function of the twist angle θ to elucidate the contributions from the simultaneously enhanced Smith–Purcell and incoherent cathodoluminescence emission. As the flatband is one-dimensional (that is, flat only along the k_y direction), the flatband-mediated Smith–Purcell radiation should reduce substantially under even a small twist of the in-plane angle θ whereas the localized incoherent cathodoluminescence should remain similar, which enables the differentiation between the two emission processes in our data. Corroborating the decomposition of the $\theta \approx 0°$ spectra in Fig. 3b–e (Supplementary Section 5C), this contrasting dependence was confirmed by the twist angle $\theta \approx \pm 5°$ measurements in Fig. 3f,g, in which the enhancement reduces to about 30-fold, lower than that in Fig. 3e. For completeness, we also performed twist-angle radiation measurement from a grating (Supplementary Section 13), which exhibited negligibly weak dependence on the twist angle, reflecting the nonresonant nature of the conventional Smith–Purcell radiation.

Furthermore, we reveal how resonance-mediated free-electron radiation can be used to control the polarization of free-electron emission. The conventional Smith–Purcell radiation has a preferred polarization parallel to the electron beam, which calls for the ability to generate and control arbitrary polarization states. Towards this direction, recent endeavours are epitomized by bianisotropic metasurfaces[34,35], albeit

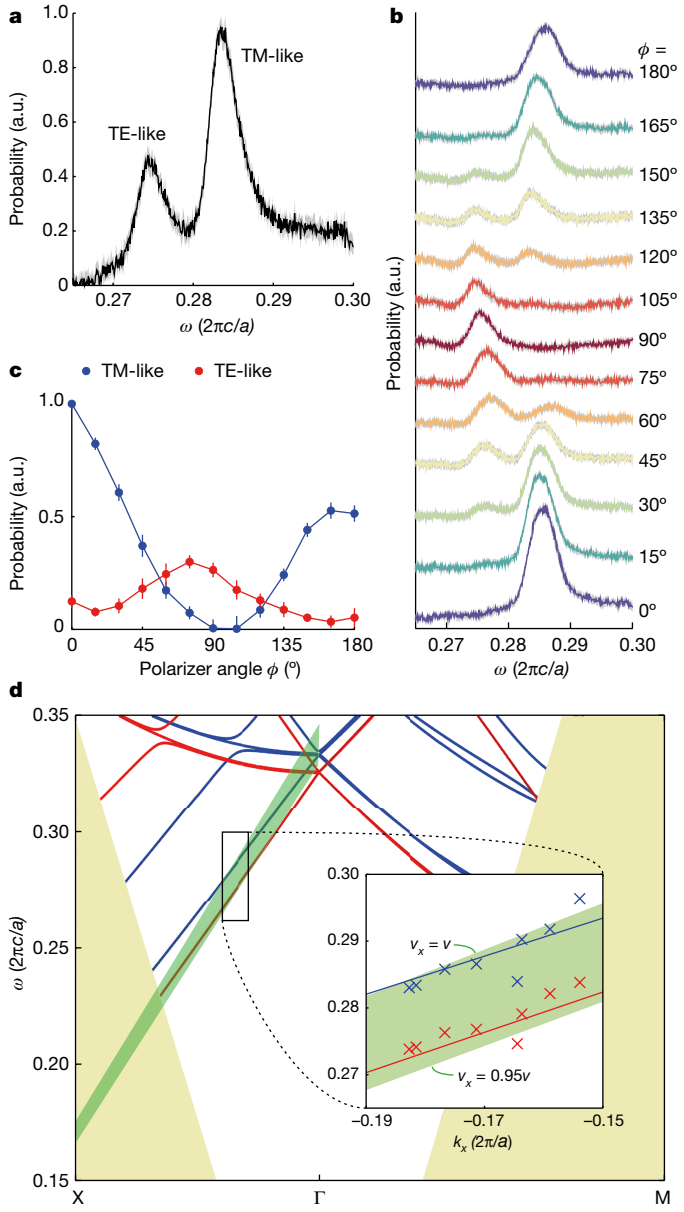

Fig. 4 | Polarization control of free-electron radiation. a,**b**, Simultaneous excitation of multiple flatbands (without the detection polarizer; **a**) and their contrasting polarization dependence (with polarizer, pass angle $\phi \in [0°, 180°]$; **b**). **c**, Peak radiation probability of the transverse-magnetic (TM)-like (blue) and transverse-electric (TE)-like (red) modes under various ϕ. **d**, Photonic bands (theory: lines) measured (crosses) with free-electron radiation by translating the field of view of the collection optics. In this set of measurements, the electron velocity is $v \approx 0.343c$. In **a**–**c**, shading and error bars indicate standard error $\pm 1\sigma$. Spectra are offset for readability in **b**. In **d**, the green shading indicates the longitudinal cut of the electron surface $\omega = vk_x$ under 5% in-plane velocity uncertainty. The areas shaded yellow are outside the light cone.

limited to the microwave regime. As our photonic crystal slab was shallowly etched, the frequency splitting between transverse-electric-like and transverse-magnetic-like bands is moderate, which enables simultaneous excitation of the two bands using free electrons at certain velocities. This is confirmed by the measured two-peak spectrum at $v \approx 0.343c$ (Fig. 4a). The two peaks correspond to different *s* and *p* far-field polarization (Fig. 4b,c)—the transverse-electric-like and transverse-magnetic-like peaks exhibited maximum emission at a polarization orthogonal and parallel to the electron beam direction, respectively (Methods).

Finally, the simultaneous excitation of the two modes enables us to measure their dispersion from their far-field radiation. As the electron surface is almost parallel to the two bands under the chosen velocity (see the bands and the electron surfaces in Fig. 4d), the overlapped photonic band structure can be extracted from the emission spectra by translating the objective's field of view (Fig. 3a and Supplementary Section 4). In the experimentally accessible region (inset in Fig. 4d) of the band structure, we observed a linear, monotonic trend of dispersion of both modes (crosses), in accordance with the calculated bands (lines).

To sum up, we have demonstrated full energy–momentum matching between free electrons and an optical environment through a continuum of flatband resonances. The flatband gives rise to strongly enhanced free-electron radiation, which also enables us to perform polarization shaping and to measure photonic bands through free electrons. The enhancement from flatband can be further improved by theoretical and experimental means. Beyond this work in which free electrons couple to one-dimensional flatband resonances, higher-dimensional flatbands[36], arcs of bound states in the continuum[37,38] and superradiance from bunched electrons could be explored to further increase the enhancement (Supplementary Section 14). Experimentally, ultrafast scanning transmission electron microscopes and integrated free-electron emitters[25,39] could provide more collimated and focused electron beams to reduce material deterioration, increase interaction duration and pinpoint the flatband coupling condition more accurately.

The flatband-mediated electron–light interaction, realized here with photonic crystals, can be generically applied to a variety of material platforms (for example, two-dimensional, plasmonic and hybrid materials; see an example on a plasmonic lattice in Supplementary Section 14) and spectral ranges (for example, terahertz, ultraviolet and X-ray generation) in both the spontaneous and stimulated regimes. Aside from enhanced far-field radiation, as observed here, the excitation of a flatband continuum can also generate strongly localized near fields (Supplementary Section 11) in transversely periodic structures—without the need to define propagation channels and thus enabling large electron fluxes—that overlap largely with and act strongly back onto free electrons, which is relevant for strong-coupling multi-photon processes[40], electron–photon coincidence measurements[41,42] and large acceleration gradients in accelerators[43–45] (also see Supplementary Section 15).

More broadly, our results highlight free electrons as pumps[46] and probes[47,48] for photonic topological bands and defects. By varying the velocity of free electrons and their twist angles relative to photonic structures, coupling with boundary modes can be realized and closed contours can be constructed in momentum space to diagnose bulk properties such as winding numbers.

Online content

Any methods, additional references, Nature Portfolio reporting summaries, source data, extended data, supplementary information, acknowledgements, peer review information; details of author contributions and competing interests; and statements of data and code availability are available at https://doi.org/10.1038/s41586-022-05387-5.

1. Baba, T. Slow light in photonic crystals. *Nat. Photon.* **2**, 465–473 (2008).
2. Noda, S., Yokoyama, M., Imada, M., Chutinan, A. & Mochizuki, M. Polarization mode control of two-dimensional photonic crystal laser by unit cell structure design. *Science* **293**, 1123–1125 (2001).
3. Rakich, P. T. et al. Achieving centimetre-scale supercollimation in a large-area two-dimensional photonic crystal. *Nat. Mater.* **5**, 93–96 (2006).
4. Park, C.-H., Son, Y.-W., Yang, L., Cohen, M. L. & Louie, S. G. Electron beam supercollimation in graphene superlattices. *Nano Lett.* **8**, 2920–2924 (2008).
5. Pellegrini, C., Marinelli, A. & Reiche, S. The physics of x-ray free-electron lasers. *Rev. Mod. Phys.* **88**, 015006 (2016).
6. De Abajo, F. G. Optical excitations in electron microscopy. *Rev. Mod. Phys.* **82**, 209 (2010).
7. Polman, A., Kociak, M. & García de Abajo, F. J. Electron-beam spectroscopy for nanophotonics. *Nat. Mater.* **18**, 1158–1171 (2019).

8. Sapra, N. V. et al. On-chip integrated laser-driven particle accelerator. *Science* **367**, 79–83 (2020).
9. Shiloh, R. et al. Electron phase-space control in photonic chip-based particle acceleration. *Nature* **597**, 498–502 (2021).
10. Friedman, A., Gover, A., Kurizki, G., Ruschin, S. & Yariv, A. Spontaneous and stimulated emission from quasifree electrons. *Rev. Mod. Phys.* **60**, 471 (1988).
11. Schächter, L. *Beam-Wave Interaction in Periodic and Quasi-Periodic Structures* (Springer, 2011).
12. de Abajo, F. G. et al. Cherenkov effect as a probe of photonic nanostructures. *Phys. Rev. Lett.* **91**, 143902 (2003).
13. Lin, X. et al. Controlling Cherenkov angles with resonance transition radiation. *Nat. Phys.* **14**, 816–821 (2018).
14. Roques-Carmes, C. et al. Towards integrated tunable all-silicon free-electron light sources. *Nature Commun.* **10**, 3176 (2019).
15. Haeusler, U., Seidling, M., Yousefi, P. & Hommelhoff, P. Boosting the efficiency of Smith–Purcell radiators using nanophotonic inverse design. *ACS Photon.* **9**, 664–671 (2022).
16. Yang, Y. et al. Maximal spontaneous photon emission and energy loss from free electrons. *Nat. Phys.* **14**, 894–899 (2018).
17. Yamaguti, S., Inoue, J.-i, Haeberlé, O. & Ohtaka, K. Photonic crystals versus diffraction gratings in Smith-Purcell radiation. *Phys. Rev. B* **66**, 195202 (2002).
18. Ochiai, T. & Ohtaka, K. Electron energy loss and Smith-Purcell radiation in two-and three-dimensional photonic crystals. *Opt. Express* **13**, 7683–7698 (2005).
19. Bendana, X., Polman, A. & de Abajo, F. J. G. Single-photon generation by electron beams. *Nano Lett.* **11**, 5099–5103 (2011).
20. Fernandes, D. E., Maslovski, S. I. & Silveirinha, M. G. Cherenkov emission in a nanowire material. *Phys. Rev. B* **85**, 155107 (2012).
21. Adamo, G. et al. Light well: a tunable free-electron light source on a chip. *Phys. Rev. Lett.* **103**, 113901 (2009).
22. Pendry, J. & Martin-Moreno, L. Energy loss by charged particles in complex media. *Phys. Rev. B* **50**, 5062 (1994).
23. So, J.-K. et al. Cerenkov radiation in metallic metamaterials. *Appl. Phys. Lett.* **97**, 151107 (2010).
24. Kaminer, I. et al. Spectrally and spatially resolved Smith-Purcell radiation in plasmonic crystals with short-range disorder. *Phys. Rev. X* **7**, 011003 (2017).
25. Liu, F. et al. Integrated Cherenkov radiation emitter eliminating the electron velocity threshold. *Nat. Photon.* **11**, 289–292 (2017).
26. Kfir, O., Di Giulio, V., de Abajo, F. J. G. & Ropers, C. Optical coherence transfer mediated by free electrons. *Sci. Adv.* **7**, eabf6380 (2021).
27. Hayun, A. B. et al. Shaping quantum photonic states using free electrons. *Sci. Adv.* **7**, eabe4270 (2021).
28. Dahan, R. et al. Resonant phase-matching between a light wave and a free-electron wavefunction. *Nat. Phys.* **16**, 1123–1131 (2020).
29. Adiv, Y. et al. Quantum nature of dielectric laser accelerators. *Phys. Rev. X* **11**, 041042 (2021).
30. Kremers, C., Chigrin, D. N. & Kroha, J. Theory of Cherenkov radiation in periodic dielectric media: emission spectrum. *Phys. Rev. A* **79**, 013829 (2009).
31. Chiu, C.-K. & Schnyder, A. P. Classification of reflection-symmetry-protected topological semimetals and nodal superconductors. *Phys. Rev. B* **90**, 205136 (2014).
32. Roques-Carmes, C. et al. A framework for scintillation in nanophotonics. *Science* **375**, eabm9293 (2022).
33. Brenny, B., Coenen, T. & Polman, A. Quantifying coherent and incoherent cathodoluminescence in semiconductors and metals. *J. Appl. Phys.* **115**, 244307 (2014).
34. Wang, Z., Yao, K., Chen, M., Chen, H. & Liu, Y. Manipulating Smith-Purcell emission with Babinet metasurfaces. *Phys. Rev. Lett.* **117**, 157401 (2016).
35. Jing, L. et al. Polarization shaping of free-electron radiation by gradient bianisotropic metasurfaces. *Laser Photon. Rev.* **15**, 2000426 (2021).
36. Tang, H. et al. Modeling the optical properties of twisted bilayer photonic crystals. *Light Sci. Appl.* **10**, 157 (2021).
37. Cerjan, A., Hsu, C. W. & Rechtsman, M. C. Bound states in the continuum through environmental design. *Phys. Rev. Lett.* **123**, 023902 (2019).
38. Cerjan, A. et al. Observation of bound states in the continuum embedded in symmetry bandgaps. *Sci. Adv.* **7**, eabk1117 (2021).
39. Guerrera, S. & Akinwande, A. I. Nanofabrication of arrays of silicon field emitters with vertical silicon nanowire current limiters and self-aligned gates. *Nanotechnology* **27**, 295302 (2016).
40. Adiv, Y. et al. Observation of 2D Cherenkov radiation. Preprint at https://arXiv.org/abs/2203.01698 (2022).
41. Feist, A. et al. Cavity-mediated electron-photon pairs. *Science* **377**, 777–780 (2022).
42. Varkentina, N. et al. Cathodoluminescence excitation spectroscopy: nanoscale imaging of excitation pathways. Preprint at https://arXiv.org/abs/2202.12520 (2022).
43. Black, D. S. et al. Net acceleration and direct measurement of attosecond electron pulses in a silicon dielectric laser accelerator. *Phys. Rev. Lett.* **123**, 264802 (2019).
44. Schönenberger, N. et al. Generation and characterization of attosecond microbunched electron pulse trains via dielectric laser acceleration. *Phys. Rev. Lett.* **123**, 264803 (2019).
45. Niedermayer, U. et al. Low-energy-spread attosecond bunching and coherent electron acceleration in dielectric nanostructures. *Phys. Rev. Appl.* **15**, L021002 (2021).
46. Fallah, A., Kiasat, Y., Silveirinha, M. G. & Engheta, N. Nonreciprocal guided waves in the presence of swift electron beams. *Phys. Rev. B* **103**, 214303 (2021).
47. Peng, S. et al. Probing the band structure of topological silicon photonic lattices in the visible spectrum. *Phys. Rev. Lett.* **122**, 117401 (2019).
48. Yu, Y. et al. Transition radiation in photonic topological crystals: quasiresonant excitation of robust edge states by a moving charge. *Phys. Rev. Lett.* **123**, 057402 (2019).

Methods

Design of flatbands in photonic crystal slabs

Flatbands emerge from various structures such as Lieb and kagome lattices[49–52], line graphs[53] and moiré superlattices[54,55]. To achieve full energy–momentum matching with point electrons, we propose to introduce a continuum of photonic modes along the transverse momenta of free electrons, which turns out to be the signature featureof flatbands. There are various ways to create photonic flatbands[56,57], such as laser-written waveguide arrays[49,50,58], photonic crystals[1,3,59], moiré structures[36,55,60–62] and their non-Hermitian counterparts[63,64]. Their applications include lasers[65,66], imaging[67] and optical communications[1]. Despite these advances, photonic flatbands have been mostly studied under pure optical settings, but never explored for electron–photon interactions. In this work, we design flatbands based on the photonic crystal platform.

The macroscopic-scale photonic crystal slab, fabricated with interference lithography, has a periodicity of $a \approx 430$ nm. The thicknesses of the device layer and the buried oxide layer are $1.19a$ and $2.38a$, respectively. The air holes of the photonic crystal slab have a radius of $r \approx 0.34a$ and a depth of $t \approx 0.13a$ (Fig. 2a). We choose to etch the air holes in this shallow manner for two reasons: first, non-Hermiticity appears only perturbatively without substantially modifying the desired dispersion of the real part of the complex frequencies (Fig. 1e,f), and therefore the effective Hamiltonian in equation (1) described above still applies; second, the frequency of the flatband resonances can be reduced for phase matching with free electrons of finite energy (≤40 keV available in our setup).

Radiation measurement

Electron beams were generated from a LaB_6 electronic gun in the high-current regime ≈30–60 μA. Space charge effects are negligible given the conditions of our electron beam (Supplementary Section 3). We chose electron velocities near v_+, rather than v_- because the electron gun produces higher-quality beams under higher voltages (Supplementary Section 3). We tuned the velocity of free electrons to form different intersections between the electron surface and the photonic band and recorded the associated radiation. The control of the in-plane, relative orientation (that is, a twist angle θ; Fig. 3a) between the photonic crystal slab and the electron beam enabled us to create radiation probability maps $P(v, \omega; \theta)$ as a function of electron velocity v and frequency ω.

In Fig. 4c, the signal reduction at polarization angle $\phi = 180°$, compared to that at $\phi = 0°$, could result from the charge accumulation on the sample under longer beam exposure, because we measured $\phi = 0–180°$ sequentially with increasing angle and with a high-current excitation.

Generation of sheet electron beams

Sheet electron beams are widely used as a mathematical convenience that reduces computational complexity in modelling free-electron radiation sources[68–72]. In reality, almost all electron sources generate point electrons; the generation of sheet electron beams is possible in principle[73–76], but is experimentally challenging, requiring electron beam shaping that relies on substantial electron optics and precise control despite space charge at high-flux configurations.

Data availability

Data supporting the findings of this study are provided in the Article and its Supplementary Information. Source data are provided with this paper.

49. Mukherjee, S. et al. Observation of a localized flat-band state in a photonic Lieb lattice. *Phys. Rev. Lett.* **114**, 245504 (2015).
50. Vicencio, R. A. et al. Observation of localized states in Lieb photonic lattices. *Phys. Rev. Lett.* **114**, 245503 (2015).
51. Slot, M. R. et al. Experimental realization and characterization of an electronic Lieb lattice. *Nat. Phys.* **13**, 672–676 (2017).
52. Kang, M. et al. Dirac fermions and flat bands in the ideal kagome metal FeSn. *Nat. Mater.* **19**, 163–169 (2020).
53. Kollár, A. J., Fitzpatrick, M., Sarnak, P. & Houck, A. A. Line-graph lattices: Euclidean and non-Euclidean flat bands, and implementations in circuit quantum electrodynamics. *Commun. Math. Phys.* **376**, 1909–1956 (2019).
54. Cao, Y. et al. Unconventional superconductivity in magic-angle graphene superlattices. *Nature* **556**, 43–50 (2018).
55. Wang, P. et al. Localization and delocalization of light in photonic moiré lattices. *Nature* **577**, 42–46 (2020).
56. Leykam, D., Andreanov, A. & Flach, S. Artificial flat band systems: from lattice models to experiments. *Adv. Phys. X* **3**, 1473052 (2018).
57. Leykam, D. & Flach, S. Perspective: photonic flatbands. *APL Photonics* **3**, 070901 (2018).
58. Tang, L. et al. Photonic flat-band lattices and unconventional light localization. *Nanophotonics* **9**, 1161–1176 (2020).
59. Li, J., White, T. P., O'Faolain, L., Gomez-Iglesias, A. & Krauss, T. F. Systematic design of flat band slow light in photonic crystal waveguides. *Opt. Express* **16**, 6227–6232 (2008).
60. Lou, B. et al. Theory for twisted bilayer photonic crystal slabs. *Phys. Rev. Lett.* **126**, 136101 (2021).
61. Dong, K. et al. Flat bands in magic-angle bilayer photonic crystals at small twists. *Phys. Rev. Lett.* **126**, 223601 (2021).
62. Nguyen, D. X. et al. Magic configurations in moiré superlattice of bilayer photonic crystal: almost-perfect flatbands and unconventional localization. Preprint at https://arXiv.org/abs/2104.12774 (2021).
63. Leykam, D., Flach, S. & Chong, Y. D. Flat bands in lattices with non-Hermitian coupling. *Phys. Rev. B* **96**, 064305 (2017).
64. Pan, M., Zhao, H., Miao, P., Longhi, S. & Feng, L. Photonic zero mode in a non-Hermitian photonic lattice. *Nat. Commun.* **9**, 1308 (2018).
65. Noda, S., Kitamura, K., Okino, T., Yasuda, D. & Tanaka, Y. Photonic-crystal surface-emitting lasers: review and introduction of modulated-photonic crystals. *IEEE J. Sel. Top. Quantum Electron.* **23**, 1–7 (2017).
66. Longhi, S. Photonic flat-band laser. *Opt. Lett.* **44**, 287–290 (2019).
67. Xia, S. et al. Unconventional flatband line states in photonic Lieb lattices. *Phys. Rev. Lett.* **121**, 263902 (2018).
68. Schächter, L. & Ron, A. Smith-Purcell free-electron laser. *Phys. Rev. A* **40**, 876 (1989).
69. Luo, C., Ibanescu, M., Johnson, S. G. & Joannopoulos, J. Cerenkov radiation in photonic crystals. *Science* **299**, 368–371 (2003).
70. Andrews, H. & Brau, C. Gain of a Smith-Purcell free-electron laser. *Phys. Rev. Accel. Beams* **7**, 070701 (2004).
71. Kumar, V. & Kim, K.-J. Analysis of Smith-Purcell free-electron lasers. *Phys. Rev. E* **73**, 026501 (2006).
72. Freund, H. & Abu-Elfadl, T. Linearized field theory of a Smith-Purcell traveling wave tube. *IEEE Trans. Plasma Sci.* **32**, 1015–1027 (2004).
73. Brinkmann, R., Derbenev, Y. & Flöttmann, K. A low emittance, flat-beam electron source for linear colliders. *Phys. Rev. Accel. Beams* **4**, 053501 (2001).
74. Piot, P., Sun, Y.-E. & Kim, K.-J. Photoinjector generation of a flat electron beam with transverse emittance ratio of 100. *Phys. Rev. Accel. Beams* **9**, 031001 (2006).
75. Nguyen, K. T. et al. Intense sheet electron beam transport in a uniform solenoidal magnetic field. *IEEE Trans. Electron Devices* **56**, 744–752 (2009).
76. Wang, Z. et al. High-power millimeter-wave BWO driven by sheet electron beam. *IEEE Trans. Electron Devices* **60**, 471–477 (2012).
77. Yang, Y. et al. Apparatus and methods for generating and enhancing Smith-Purcell radiation. US patent 10,505,334 (2019).

Acknowledgements We thank T. Savas for fabricating the samples; A. Massuda and J. Sloan for contributions to the building of the setup; D. Zhu and M. Lončar for sharing equipment; and C. Mao, O. D. Miller and N. Rivera for stimulating conversations. This material is based on work supported in part by the US Army Research Office through the Institute for Soldier Nanotechnologies under contract number W911NF-18-2-0048, the Air Force Office of Scientific Research under the award numbers FA9550-20-1-0115 and FA9550-21-1-0299, the US Office of Naval Research Multidisciplinary University Research Initiative grant N00014-20-1-2325 on Robust Photonic Materials with High-Order Topological Protection, and the U.S.-Israel Binational Science Foundation grant 2018288. Y.Y. acknowledges the support from the start-up fund of the University of Hong Kong and the National Natural Science Foundation of China Excellent Young Scientists Fund (HKU 12222417). C.R.-C. acknowledges funding from the MathWorks Engineering Fellowship Fund by MathWorks Inc.

Author contributions Y.Y., C.R.-C., I.K. and M.S. conceived the project. Y.Y. designed the sample. C.R.-C. and S.E.K. performed the radiation measurements. H.T. and Y.Y. performed the Fourier scattering spectroscopy. J.B. designed and fabricated the objective motorized stage with inputs from C.R.-C. and S.E.K. Y.Y. and C.R.-C. analysed the data. Y.Y. and C.R.-C. wrote the manuscript with inputs from all authors. E.M., I.K., J.D.J. and M.S. supervised the project.

Competing interests Y.Y., C.R.-C., S.E.K., I.K., J.D.J. and M.S. declare the following patent: US patent 10,505,334 (ref. [77]).

Additional information

Supplementary information The online version contains supplementary material available at https://doi.org/10.1038/s41586-022-05387-5.

Correspondence and requests for materials should be addressed to Yi Yang or Charles Roques-Carmes.

Peer review information *Nature* thanks Fang Liu and the other, anonymous, reviewer(s) for their contribution to the peer review of this work.